

Microstructure and properties of Si_3N_4 - MoSi_2 composites

D. Sciti, S. Guicciardi and A. Bellosi*

CNR-ISTEC, Institute of Science and Technology for Ceramics, Via Granarolo 64, I-48018 Faenza, Italy

Si_3N_4 -composite materials containing different amounts of MoSi_2 were produced by hot-pressing. MoSi_2 particles (mean size 0.8 μm) were homogeneously dispersed within a nanostructured Si_3N_4 matrix (mean grain size < 0.2 μm). The influence of MoSi_2 inclusions on the microstructure, and electrical and mechanical properties of the composites is discussed and compared to the properties of monolithic Si_3N_4 . As a result of the refined matrix microstructure and presence of ductile inclusions, these materials possess good mechanical properties, with bending strengths up to 1130 MPa (RT) and 880 MPa (1000°C) and fracture toughnesses up to 8 $\text{MPa}\cdot\text{m}^{1/2}$. Electrical resistivity is $\sim 10^{-3} \Omega\cdot\text{cm}$.

Key words: molybdenum disilicide, composites, microstructure, mechanical properties.

Introduction

Silicon nitride and molybdenum disilicide have recently attained considerable attention as matrix and/or reinforcing phase for the development of high performance structural or functional ceramic composites [1-17].

Molybdenum disilicide is an excellent structural and electroconductive ceramic that, due to its unique combination of properties, fulfils many of the requirements for high temperature applications [1-3]. Its moderate density (6.31 g/cm^3) is suitable for the rotating parts of turbine and automobile engines. The occurrence of a surface glassy layer of silica that forms at high temperature under oxidizing conditions ensures the excellent oxidation resistance of this material, providing improved efficiency for applications in heat exchangers and gas burners. Moreover, MoSi_2 possesses a high melting point (about 2030°C), and its high electrical conductivity can be exploited in a wide range of electrical applications such as heaters and igniters. The main limitations of this material are the low fracture toughness at room temperature and the brittle-to-ductile transition at about 1000°C. Above this temperature, the material plastically deforms and the strength values are low.

The efforts to improve the qualities of MoSi_2 have been focused on compositing. There is plenty of literature indicating various strategies of compositing where the MoSi_2 is used as the matrix or reinforcement in combination with SiC, SiAlON, Al_2O_3 , ZrO_2 and Si_3N_4 [4-17].

In this paper attention is focused on silicon nitride-

molybdenum disilicide particulate composites. Silicon nitride is one of the most important structural ceramic materials because of its combination of high-temperature refractoriness, high strength, low thermal expansion coefficient, low density and high-temperature oxidation resistance. Silicon nitride is difficult to densify due to its low diffusion coefficient. Conventionally fully dense materials can be obtained through liquid-phase sintering with the addition of sintering aids. MgO has been extensively used as a sintering aid for Si_3N_4 as well as other metal oxides, rare earth oxides and their combinations [18, 19]. The addition of MoSi_2 can further improve the performance of Si_3N_4 , especially if a suitable control of the morphology, particle size and degree of dispersion of the second phase is performed. An important factor is the amount of MoSi_2 : if it is higher than about 30 vol %, the resulting composite is electroconductive. This is advantageous from different point-of-views: on the one hand the materials associate electroconductive functions to enhance its thermo-mechanical behaviour, on the other hand complex shapes can be made by electrodischarge machining starting from simple shaped pieces. In fact, one of the main limitations of silicon nitride is the high cost of its machining. As Si_3N_4 is an electrical insulator and a hard material, it must be diamond machined, which is a time consuming and expensive process. For this reason, the addition of MoSi_2 particles allows the production of complex shapes by way of electrodischarge machining, which is a relatively low-cost technique. Moreover, it has been found that MoSi_2 additions can improve oxidation resistance and fracture toughness compared to monolithic silicon nitride [9].

In this paper, composites containing different amounts of MoSi_2 were produced by hot-pressing. Alumina and yttria are the additives selected for the densification of Si_3N_4 . This system ($\text{Si}_3\text{N}_4 + \text{Al}_2\text{O}_3 + \text{Y}_2\text{O}_3$) has been

*Corresponding author:
Tel : +39 0456 699711
Fax: +39 0546 46381
E-mail: irtec@irtec1.irtec.bo.cnr.it

studied previously and picked as the matrix for the present composite materials due to its high sinterability and excellent mechanical properties such as fracture toughness and flexural strength [18, 19].

The microstructure and properties of the composites were compared to those of the matrix in order to investigate the origin of the toughening and strengthening mechanisms due to the action of the MoSi₂ particles. Thermal and electrical properties were also measured and are discussed.

Experimental

Commercial powders were used as raw materials. Their main characteristics are indicated below.

- Si₃N₄ powder (Ube-SN-E10): 95% α-Si₃N₄ and 5% β-Si₃N₄, specific surface area: 11.5 m²/g, mean particle size: 0.16 μm, chemical composition: O: 1.09%, Cl: 0.01%, Fe: 0.01%, Ca: 0.005%, Al: 0.005%;
- MoSi₂ (Aldrich): purity 99%, mean particle dimensions 2.7-2.8 μm, crystalline phase: tetragonal MoSi₂.

As sintering aids for the Si₃N₄ matrix, Al₂O₃ Ceralox HPa0.5 and Y₂O₃ HC-Starck, were selected.

The following compositions were prepared:

1. 70 vol % (89 wt % Si₃N₄ + 3 wt % Al₂O₃ + 8 wt % Y₂O₃) + 30 vol % MoSi₂, labelled S30
2. 60 vol % (89 wt % Si₃N₄ + 3 wt % Al₂O₃ + 8 wt % Y₂O₃) + 40 vol % MoSi₂, labelled S40.

The powders were mixed through ball milling using Si₃N₄ balls for 24 h in ethyl alcohol. Then they were dried using a rotary evaporator and sieved. Sintering was performed by hot-pressing at 1720-1740°C with an applied pressure of 30 MPa and a holding time 10 minutes, in vacuum. The final densities were determined using Archimedes method.

All samples were examined by X-ray diffraction (XRD) to determine the crystalline phases present. The specimens were cut, polished and etched in a O₂/CF₄ plasma. The microstructures were observed by scanning electron microscopy and energy dispersive spectroscopy (SEM-EDS); micrographs of selected samples were analysed by image analysis (Image Pro-plus 4.0, Media Cybernetics, Silver Springs, USA) to determine the size distribution of MoSi₂ inclusions. The mean diameter of the inclusions was determined as the average of 500-1000 particles, depending on the sample. Each mean value is calculated by the image analysis program, as the average length of diameters measured at 2 degree intervals and passing through the particle centroid. The standard error of the mean value was taken as the ratio $standard\ deviation/\sqrt{N}$, where N is the number of grains counted. The mean grain size

and aspect ratio of the Si₃N₄ matrix particles were also determined on micrographs of plasma etched surfaces by image analysis.

On polished surfaces, Vickers microhardness (HV) was measured with a load of 9.81 N, using a Zwick 3212 tester.

Fracture toughness (K_{IC}) was evaluated by indentation crack length using a load of 98.1 N and by the chevron-notched beam (CNB) in flexure. For the indentation tests, at least ten indentations were made and the crack length measured. The formula proposed by Anstis *et al.* [20] was used for the calculation. For the chevron-notched beams, the bars, 25×2.5×2 mm³ (length × thickness × width, respectively) were notched with a 0.08 mm diamond saw; α₀ and α₁ were about 0.12 and 0.80, respectively. The flexural tests were performed on a semi-articulated alumina four-point jig with a lower span of 20 mm and an upper span of 10 mm on an Instron model 1195 universal screw-type testing machine. The specimens, three for each composition, were deformed with a crosshead speed of 0.05 mm/minute. The “slice model” equation of Munz *et al.* [21] was used for the calculation of K_{IC}.

Young modulus (E) was measured by resonant frequency on specimens 28×8×0.8 mm³ using an Hewlett Packard gain-phase analyser.

Flexural strength (σ), up to 1300°C, was measured with an Instron model 6025 screw-type testing machine, on chamfered bars 25×2×2.5 mm³ (length × thickness × width), in 4-point bending with 20 mm and 10 mm as outer span and inner span, respectively, using a crosshead speed of 0.5 mm/minute. For high temperature tests, a soaking time of 18 minutes was set to reach thermal equilibrium before starting the test.

The linear thermal expansion coefficient was measured from dilatometric tests up to 1400°C using a heating rate of 5 K/minute.

The electrical resistivity measurements were carried out using a four probe DC method at room temperature, inducing a current in bar specimens of 2×2.5×25 mm³. The current and the voltage reading were detected at the same time in two different digital high-resolution multimeters. The resistivity values were determined from the electrical resistance measurement, taking into account the test leads length and cross sectional area of the samples.

Using a Zwick indenter, cracks were also generated on polished sample surfaces in order to study the crack paths, through SEM analysis.

All the properties of the composites were compared with those of the material constituting the matrix (reported in detail in previous papers [18, 19]):

89 wt % Si₃N₄ + 3 wt % Al₂O₃ + 8 wt % Y₂O₃, labelled S0.

Table 1. Compositions, sintering conditions, density and microstructural parameters, mean \pm standard error when appropriate

Sample	Composition	Hot pressing Conditions	Density Exp. Relative (g/cm^3) %	Crystalline phases	Matrix mean Grain size (μm)	Matrix Grain Aspect ratio	MoSi_2 mean Grain size (μm)	MoSi_2 aspect ratio
S0* (reference material)	89 wt % Si_3N_4 + 3 wt % Al_2O_3 + 8 wt % Y_2O_3	1710°C/60'/30 MPa	3.30 100	β - Si_3N_4 residual α - Si_3N_4 : 7% vol	0.43 \pm 0.08	6.8	–	–
S30	70 vol % (89 wt % Si_3N_4 + 3 wt % Al_2O_3 + 8 wt % Y_2O_3) + 30 vol % MoSi_2	1720°C/10'/30 MPa	4.07 97.5	α - Si_3N_4 , β - Si_3N_4 , Tetr. MoSi_2 Traces: Hex. MoSi_2 residual α - Si_3N_4 : 40% vol	0.18 \pm 0.05	1.7	0.82 \pm 0.03	1.7
S40	60 vol % (89 wt % Si_3N_4 + 3 wt % Al_2O_3 + 8 wt % Y_2O_3) + 40 vol % MoSi_2	1740°C/10'/30 MPa	4.37 97.5	α - Si_3N_4 , β - Si_3N_4 , Tetr. MoSi_2 Traces: Hex. MoSi_2 residual α - Si_3N_4 : 36% vol	0.20 \pm 0.04	1.7	0.80 \pm 0.04	1.7

*From previous work: [18, 19]

Results and Discussion

Microstructural features of the composites (S30 and S40)

All the materials reached nearly full density after the hot-pressing route, as confirmed by the absence of porosity ascertained through microstructural analyses. The theoretical density values of the composites (Table 1) are overestimated as they were calculated on the basis of the rule of mixtures without taking into account glassy grain boundary phases. In the composites, glassy phases are present in an amount higher than in the reference monolithic material owing to some silica in the starting powder mixtures introduced with the addition of MoSi_2 particles. The presence of an amorphous SiO_2 phase is generally unavoidable in MoSi_2 , as a result of the thermodynamic stability of this phase. A 1-2% content of oxygen in the MoSi_2 powder is reported by many authors [12, 13]. In the present work, an amount of 1-2% of silica in the final products is enough to explain the deviation of experimental densities from theoretical ones.

In the composites, both α - and β - Si_3N_4 and tetragonal MoSi_2 are present. No reaction occurred between MoSi_2 and Si_3N_4 as already reported in the literature [1, 7, 9]. The diffractograms for the plane perpendicular to the hot pressing direction revealed a preferred orientation of MoSi_2 crystallites along the direction (hk0) of about 13%. By contrast, in any plane parallel to the hot pressing direction, the inclusions were randomly oriented.

In Fig. 1, an example of the fracture surface of a composite (sample S40) is shown. In spite of the difference between thermal expansion coefficients, (MoSi_2 : $9 \cdot 10^{-6} \text{ K}^{-1}$, Si_3N_4 : $3 \cdot 10^{-6} \text{ K}^{-1}$), good adhesion was found between the two phases. No pull-out of MoSi_2 particles was observed on the fracture surfaces and, according to Ref. 7, no cracks arising from thermal expansions mismatch were found on polished surfaces (Fig. 2a, b) along phase boundaries.

Fig. 2a, b also reveals the distribution, shape and

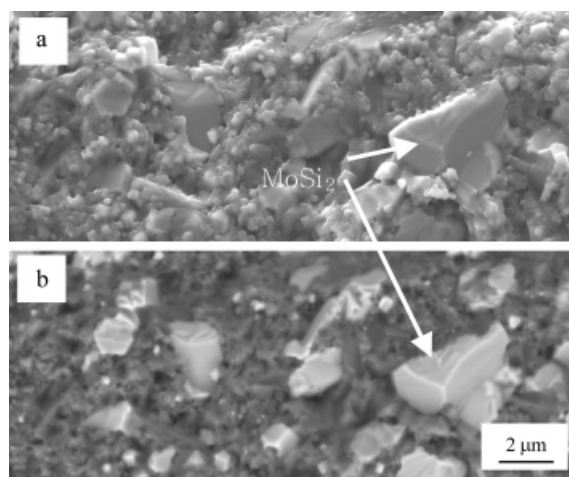


Fig. 1. Fracture surface of composite S40. (a) Secondary electron image (SE) and (b) corresponding back-scattered electron image (BSE).

dimensions of the MoSi_2 inclusions, which present a lighter contrast than the silicon nitride matrix. The composites exhibit a defect free microstructure, without residual porosity. The shape of inclusions is irregular (Fig. 2c), as their external outline follows the Si_3N_4 grain boundaries. It can be hypothesized that the higher ductility of MoSi_2 compared to the matrix material favours the constraint and the accommodation of these particles in the spaces available among Si_3N_4 grains during sintering. Moreover, due to the effect of the applied pressure, the shape is slightly elongated with the major axis perpendicular to the direction of the pressure.

The MoSi_2 mean particle diameter ($\sim 0.8 \mu\text{m}$, Table 1) and particle size distributions in the two dense composites are very similar, Fig. 3. An 80% proportion of the particles has dimensions ranging between 0.1 and $1 \mu\text{m}$, (50% of inclusions have sizes in the $0.4 \mu\text{m}$ range). Although some big particles are evident on SEM micrographs (Fig. 2a, b), higher magnification micrographs (Fig. 2c) confirm that most MoSi_2 particles have very small dimensions.

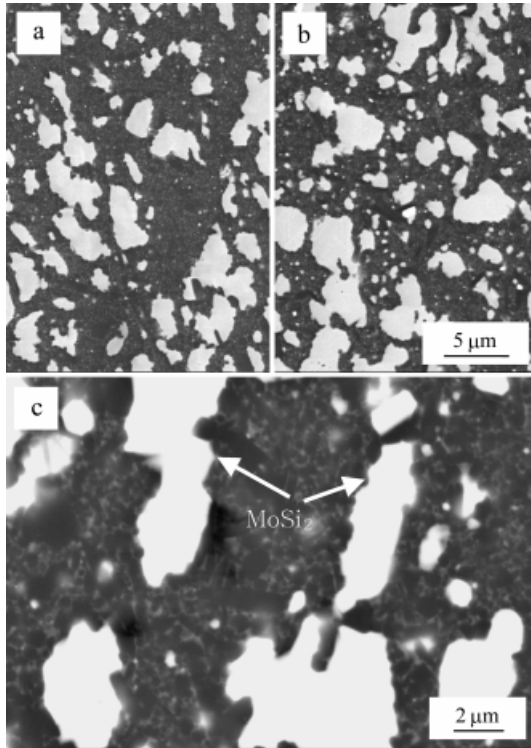


Fig. 2. Polished surface of composites. BSE image of (a) and (c) S30, (b) S40.

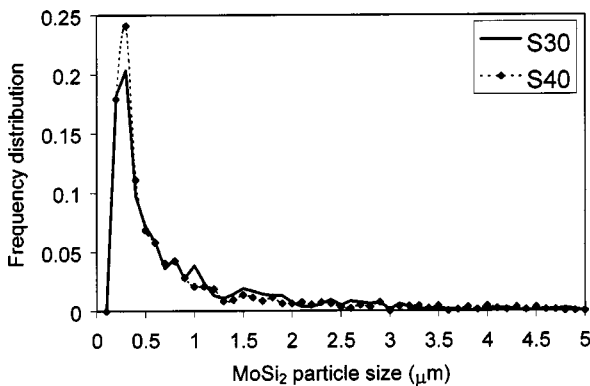


Fig. 3. Particle size distributions in the composites.

Comparing the size distribution determined by image analysis with the particle size distribution of the starting MoSi_2 powder, (the cumulative distribution shows that only 10% of the powder particles have a particle size $< 1 \mu\text{m}$), it can be concluded that MoSi_2 particles did not aggregate during the preparation of powder mixtures. This effect, already observed [7], may be due to the milling procedure.

Comparison with the microstructure of S0

In Fig. 4, an image of S40 after plasma etching is shown, revealing the microstructure of the silicon nitride matrix. The silicon nitride grain size here is considerably smaller when compared to the reference

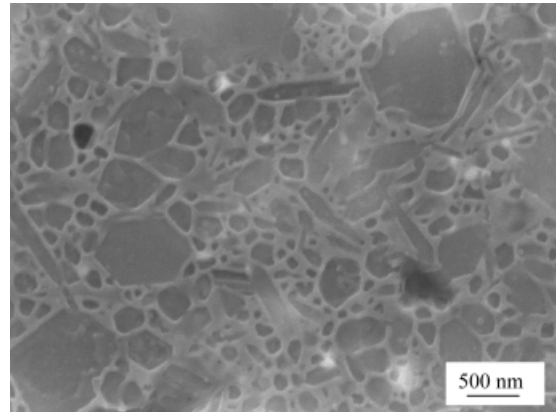


Fig. 4. Matrix microstructure after plasma etching.

material S0 (from 0.43 [19] to 0.18-0.20 μm), see Table 1.

Unlike the S0 material, the composites undergo only a partial $\alpha \rightarrow \beta$ -phase transition, as already observed in X-ray spectra: residual amounts of $\alpha\text{-Si}_3\text{N}_4$ are in the range 35-40%, Table 1. As a result, most of the Si_3N_4 grains in S30 and S40 specimens are still equiaxed. A small amount of elongated grains are also present with different aspect ratio values (up to ~ 5). The grains are separated by an intergranular secondary phase typical of liquid-phase sintered systems [18, 19], that is completely glassy, as confirmed by the absence of crystalline phases in addition to silicon nitride and molybdenum disilicide.

A direct comparison of the densification behaviour of the three samples reveals that, although the sintering temperature was about the same, the holding time (10 minutes) needed for S30 and S40 to reach a full density was considerably lower than for S0 (60 minutes). Therefore, we concluded that the presence of MoSi_2 did not inhibit densification. The low degree of several concurrent phenomena such as Si_3N_4 grain growth, the $\alpha \rightarrow \beta$ phase transition and development of Si_3N_4 elongated grains has to be ascribed primarily to the short soaking time at 1700°C. In addition, the presence of silica in the starting MoSi_2 powder must have lowered the temperature at which the liquid phase starts to form (from 1500°C for S0 to about 1400°C for S30 and S40), which means a lower viscosity of the liquid phase at the hot-pressing temperature. It is well known that the densification of silicon nitride occurs by the dissolution of $\alpha\text{-Si}_3\text{N}_4$ and its reprecipitation as $\beta\text{-Si}_3\text{N}_4$ through diffusion in the liquid phase of the involved species. The diffusion rates depend to a great extent on the liquid phase viscosity: in the case of the present composites, higher diffusion rates are associated with the lower liquid phase viscosity that favours the development of mainly equiaxed grains and lowers the aspect ratio of the elongated ones.

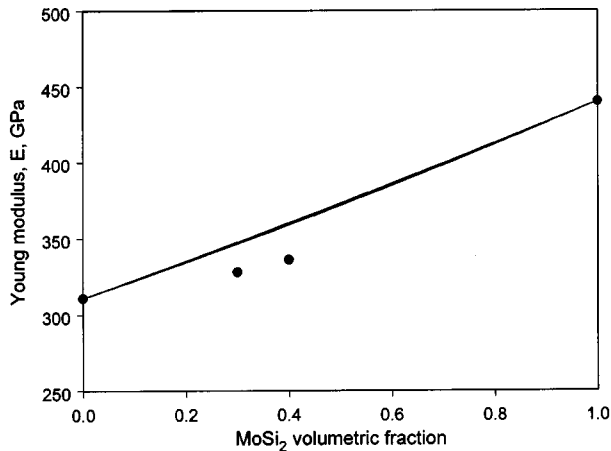


Fig. 5. Young modulus experimental values compared with Hashin and Shtrikman bounds.

Mechanical properties

1) Young modulus

In Fig. 5, the data are plotted with the Hashin and Strikman bounds [22] calculated with 440 GPa, 0.15 [1], 311 GPa, and 0.28 [23] as Young modulus and Poisson ratio for MoSi_2 and Si_3N_4 , respectively. The experimental error is estimated to be about 1%. The difference between the bounds and the experimental values of the composites can be attributed to the presence of a glassy phase, since no porosity or microcracking was observed in the microstructure. Since the contribution of the grain boundary glassy phase due to the sintering aids is already incorporated in the value relative to the reference material, a rough estimate of the additional glassy phase content coming from the introduction of the MoSi_2 can be carried out working backwards with the Hashin and Strikman bounds. Assuming the simplified hypothesis that this glassy phase is fused silica and taking 70 GPa [24] and 0.16 [25] as the Young modulus and Poisson ratio for this phase, a volumetric SiO_2 content in the range 2-4 vol % and 3-5 vol % can be calculated for S30 and S40, respectively, which are not far from some estimates of SiO_2 content in the MoSi_2 materials obtained by other methods [3, 12, 13].

2) Hardness

The Vickers hardness of the composites is in good agreement with the values found in literature on similar materials [8]. Being softer than the Si_3N_4 matrix, the introduction of the MoSi_2 phase lowers the hardness linearly [26]. As shown in the plot of Fig. 6, an estimate of MoSi_2 pure phase hardness is, by linear regression, 12.3 GPa, close to the range 9.3-11.2 GPa reported in Ref. 3.

3) Fracture toughness

Independently of the technique used, two features are

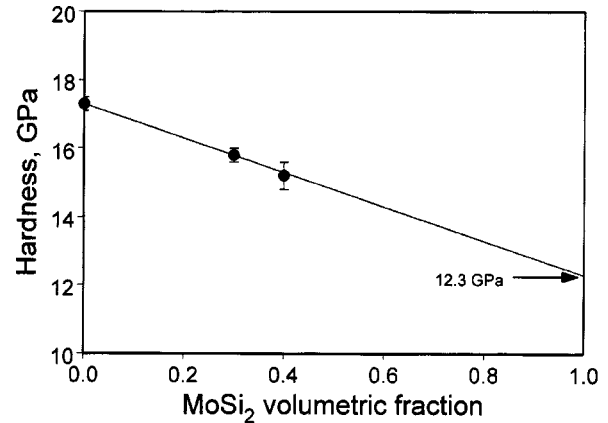


Fig. 6. Mean hardness values as a function of MoSi_2 volumetric content. The solid line is the best fit calculated on the data. Error bars are ± 1 standard deviation.

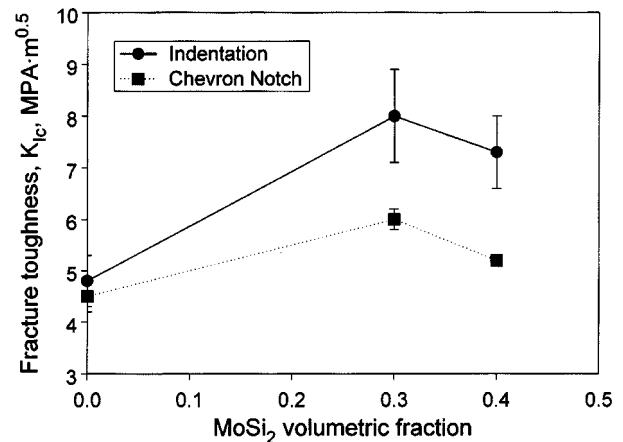


Fig. 7. Experimental fracture toughness values as measured by indentation crack length and chevron-notched beam methods. Error bars are ± 1 standard deviation.

evident from the toughness values: the increase of the K_{Ic} with the introduction of the MoSi_2 phase and the decrease of toughness when the molybdenum content passes from 30 to 40 vol %, as revealed in Fig. 7. For all the materials, the indentation fracture toughness is higher than that measured by chevron-notched beams, especially for the composites. In Ref. 8, the indentation fracture toughness values were instead found to be lower than those measured by the controlled-surface flaw method and the authors suggested that this was a possible manifestation of an R-curve phenomenon in these materials. With the configuration adopted, in our chevron-notched specimens the propagation of the crack before the unstable fracture was about 500 μm , while in the indentation toughness the length of the cracks was in the range 90-130 μm . Either an R-curve phenomenon is not so evident in our materials or it is masked by some other effects. The toughening increment due to the introduction of MoSi_2 reinforcement in the Si_3N_4 matrix was attributed by Petrovic *et al.* [8] to the residual stresses caused by the different thermal

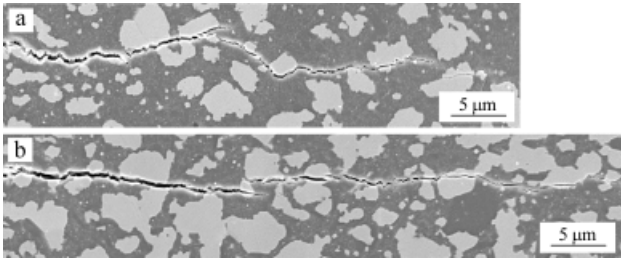


Fig. 8. Examples of crack path in (a) S30 and (b) S40.

expansion coefficients of matrix and particles.

A typical indentation crack path in the S30 and S40 materials is shown in Fig. 8 a and b, respectively. In S30, the crack path is tortuous with the fracture mainly located at the interface between the Si_3N_4 matrix and the MoSi_2 particle. The ratio of transphase/interphase fracture of the crack, calculated as the ratio between the portion of crack path cutting through the MoSi_2 phase and the portions of the crack path along the MoSi_2 - Si_3N_4 phase boundaries, ranges from 0.1 to 0.6. An interesting finding of this investigation, which deserves a deeper insight, is that the crack seems to be attracted by the particle/matrix interface while it should be repelled by virtue of the elastic moduli and thermal expansion coefficients combination between the MoSi_2 particle and the Si_3N_4 matrix [27, 28]. In S40, the crack path is less tortuous than in S30 and the fracture is mainly through the MoSi_2 particles. In this composite, the ratio of transphase/interphase fracture ranges between 1.5 and 2. It is likely that when the interparticle distance is below a critical value it becomes advantageous for the crack, due to energy considerations, to pass through the reinforcing phase instead of going around it. Since the MoSi_2 particles are less tough than the Si_3N_4 phase, this causes an overall toughness decrement [8].

In contrast to what was reported by Petrovich *et al.* [8], intact ligaments left behind the crack tip were observed in both composites, more evidently in S40

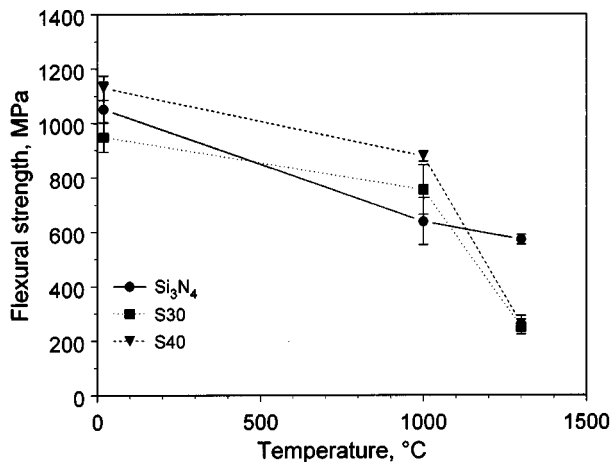


Fig. 9. Flexural strength as a function of test temperature. Error bars are ± 1 standard deviation.

than in S30, Fig. 8. These ligaments are formed by Si_3N_4 grains and MoSi_2 particles. The MoSi_2 ligaments, moreover, appear as plastically deformed zones. The presence of intact ligaments behind the crack tip may be an indication of toughening mechanisms like crack bridging or crack pinning.

4) Flexural strength

In Fig. 9, the flexural strength is plotted as a function of the test temperature and MoSi_2 content. Good values were measured, especially in the case of sample S40 with a room temperature strength of 1130 MPa, this value being slightly better than those of the starting matrix, while S30 was weaker.

The fracture origin was investigated on fracture surfaces. One example of the flaws that could have acted as critical defects is shown in Fig. 10. EDS analysis revealed that these defects are mainly Al silicates or Al-Y silicates. In the case of sample S40 the critical flaws are supposed to be much smaller as their presence on the fracture surface is more difficult to ascertain. However, some small defects containing silica were detected on the fracture surface. Molybdenum disilicide does not seem to play any role in such defects, indicating good homogeneity in the dispersion of the second phase.

An estimation of the critical flaw size can be computed according to:

$$\sigma = \frac{1K_{Ic}}{y\sqrt{c}} \quad (1)$$

where σ is the flexural strength, y a constant equal to 1.29 for a small penny-shape surface flaw [29], K_{Ic} the fracture toughness and c the flaw radius. The values of c for the composites, according to eq. (1), are 24 μm and 13 μm , respectively for the composites S30 and S40 which agrees well with microstructural observations (Fig. 10).

Comparing the strength values of the composites

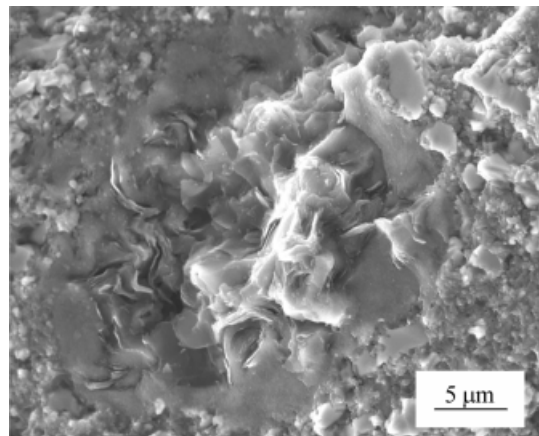


Fig. 10. Example of critical flaw on S30 fracture surface (RT strength test).

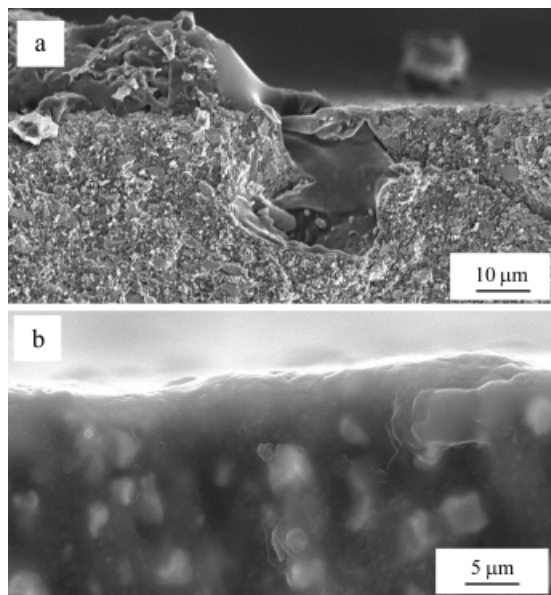


Fig. 11. (a) Critical flaw in S30, strength test at 1000°C. A viscous glass flowed into the flaw. (b) Oxidation layer on S40 fracture surface after strength test at 1300°C.

with the reference Si_3N_4 , it was concluded that the slight improvement of strength in S40 can be attributed to the decrease of matrix grain size and the increase of toughness. In S30, a similar behaviour was expected, but a lack of proper control of the glassy phase distribution led to the formation of critical defects whose effect might have overcome the beneficial effects of toughness improvement and fine matrix microstructure.

At 1000°C, the flexural strength decreases both for the matrix and the composites. The material S40, which remains stronger than the matrix, has a remarkable value of about 900 MPa. The strength decrease is lower for the composites (about 20%) than for the matrix (about 40%). At this temperature, the load-displacement curves of the composites show some non-linearity, as previously observed [8, 30]. At 1300°C, a pronounced decrease is observed for the composites (250-260 MPa, corresponding to a decrease of 70-80% compared to the initial value), while the monolithic Si_3N_4 strength is as high as 571 MPa (strength decrease 45%). The dominant deformation mechanism in Si_3N_4 at high temperature is grain boundary softening which promotes subcritical crack growth and then a strength decrease. In the composites, the grain boundary softening of the matrix is accompanied also by the plastic deformation of the MoSi_2 particles [8] which reduces the flexural strength even more.

An additional feature of high temperature strength tests, is oxidation, due to exposure to the air. A thin layer of glassy silicates containing a concentration of additive cations and other impurities formed on the bar surfaces, with a thickness ranging from few micrometres to about 20 μm . The morphology of this layer indicated that above 1000°C the viscosity of this surface

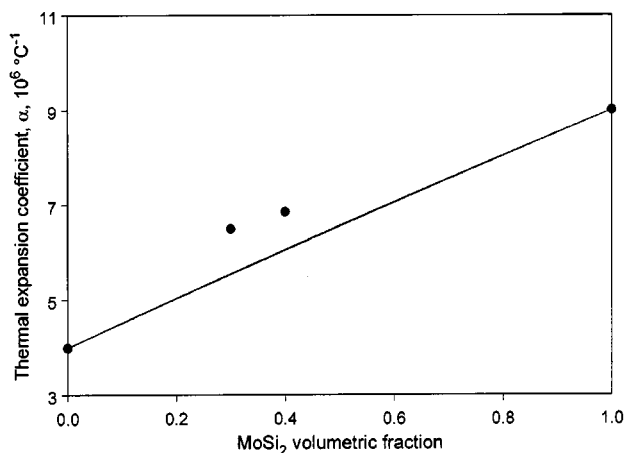


Fig. 12. Experimental values of thermal expansion coefficients compared with theoretical bounds.

oxide was rather low, as it flowed and concentrated in some parts of the test bar or even inside the surface defects (Fig. 11a). Further, the fracture surfaces were covered by a very thin glassy layer (Fig. 11b), as, during crack propagation, new surfaces were created and exposed to the oxidizing environment.

Linear thermal expansion behaviour

The experimental values obtained (6.50 and $6.86 \cdot 10^{-6} \text{ K}^{-1}$ for S30 and S40, respectively) are shown in Fig. 12 as a function of the MoSi_2 content. This data is compared to the theoretical limits [31] calculated with the following parameters: Si_3N_4 Young modulus = 311 GPa, Si_3N_4 Poisson ratio = 0.28 [23], MoSi_2 Young modulus = 440 GPa [1], MoSi_2 Poisson ratio = 0.15 [1], Si_3N_4 thermal expansion coefficient = $3.51 \cdot 10^{-6} \text{ K}^{-1}$, MoSi_2 thermal expansion coefficient = $9 \cdot 10^{-6} \text{ K}^{-1}$.

The values obtained from this calculation are $5.54 \cdot 10^{-6} \text{ K}^{-1}$ and $5.56 \cdot 10^{-6} \text{ K}^{-1}$ as lower and upper value for S30, $6.05 \cdot 10^{-6} \text{ K}^{-1}$ and $6.07 \cdot 10^{-6} \text{ K}^{-1}$ for S40.

The deviation from the theoretical models is not understood at this moment.

If the contribution of glassy phase is considered, the agreement between experiment and theory does not improve as thermal expansion coefficients of glasses are very low (in the case of glasses in the system $\text{SiO}_2\text{-Al}_2\text{O}_3$, it ranges from $1.45\text{-}2.27 \cdot 10^{-6} \text{ K}^{-1}$ [32]).

Electrical resistivity

Both composites are good conductors with resistivities of the order $10^{-3} \Omega\text{-cm}$, as a result of interconnectivity of MoSi_2 inclusions. In the work of Kao [9] an Si_3N_4 composite containing 30 vol % of MoSi_2 exhibited a resistivity two orders of magnitude higher than sample S30. This difference is related to the mean dimensions of the conductive particles that in the present case are at least one order of magnitude smaller than in the work mentioned. The experimental values confirmed that 30 vol % of MoSi_2 is well over the

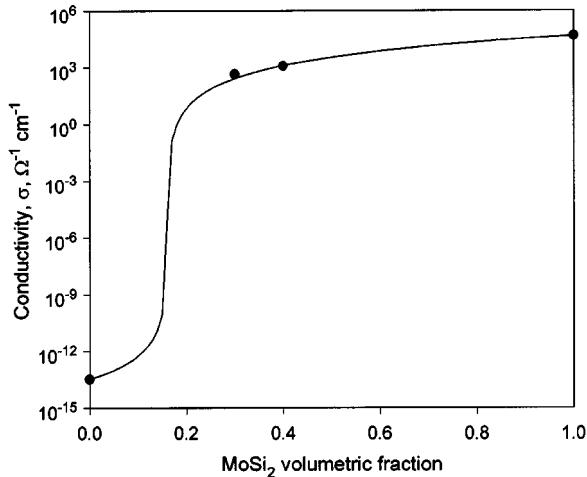


Fig. 13. Experimental values of electrical conductivity compared with percolation theory. Data are fitted with a t value of 2.89 (see text).

percolation limit for conductivity.

The data obtained were compared to the theoretical models proposed in the literature for the electrical resistivity of composite systems. As the materials of the present study are near to the insulator-conductor transition, the percolation theory applies [33].

The experimental data were fitted according to the equation proposed by McLachlan *et al.* [33]:

$$\frac{f(\sigma_m^{1/t} - \sigma_{comp}^{1/t})}{\sigma_m^{1/t} + A\sigma_{comp}^{1/t}} + \frac{(1-f)(\sigma_p^{1/t} - \sigma_{comp}^{1/t})}{\sigma_p^{1/t} + A\sigma_{comp}^{1/t}} = 0 \quad (2)$$

where f is the volume fraction of the conductive particles, σ_{comp} is the conductivity of the composite, A is $f_c/(1-f_c)$ with f_c the percolation threshold (0.16 for a 3-D spherical particle arrangement [33]), σ_m , σ_p are the conductivities of the matrix and particle, respectively, and t an adjustable exponent with values in the range 1-4.49. The results are shown in Fig. 13 where the agreement between experiment and theory seems to be quite good for a t value of 2.89.

Conclusions

Composites of Si_3N_4 - MoSi_2 containing different amounts (30 and 40 vol %) of MoSi_2 with alumina and yttria as sintering aids were produced by hot-pressing and their microstructure and properties were studied and compared to those of the Si_3N_4 constituting the matrix.

The presence of MoSi_2 inhibited the Si_3N_4 grain growth, the development of elongated grains and the $\alpha \rightarrow \beta$ - Si_3N_4 phase transition without retarding densification. As a result, an ultrafine matrix was obtained with a mean grain size of about 0.2 μm .

The combination of the fine microstructure of the matrix Si_3N_4 with the presence of the MoSi_2 particles was beneficial for almost all the mechanical properties,

including fracture toughness and mechanical strength. Both these properties were discussed in terms of the microstructural features of the composites and the agreement of the properties with different models were assessed. In addition, the composite samples were good conductors with resistivities of the order $10^{-3} \Omega\text{-cm}$. Electrical conductivity resulted from the contact of MoSi_2 inclusions, whose volume fraction is over the percolation limit for both the composites produced.

High temperature properties were affected by the type and amount of grain boundary phases, therefore the residual silica in the initial MoSi_2 powder has a negative influence on strength above 1000°C.

Acknowledgements

The Authors wish to thank their co-workers Gualtiero Fabbri for electrical resistance measurements, Cesare Melandri for mechanical tests, Daniele dalle Fabbrie for technical assistance, Elena Landi for the useful discussion on thermal expansion behaviour.

References

1. Y.-L. Jang, and E.J. Lavernia, *J. Mat. Sci. Lett.* 29 (1994) 2557-2571.
2. J.J. Petrovic, and A.K. Vasudevan, *Mat. Sci. and Eng. A* 261 (1999) 1-5.
3. Newmann, T. Jewett, S. Sampath, C. Bernt, and H. Herman, *J. Mat. Res.* 13[9] (1998) 2662-2671.
4. J. Pan, M.K. Surappa, R.A. Saravanan, B.W. Liu, and D.M. Yang, *Mat. Sci. Eng. A244* (1998) 191-198.
5. A. Newman, S. Sampath, and H. Herman, *Mat. Sci. Eng. A261* (1999) 252-260.
6. L.O. Nordberg, and T. Ekström, *J. Am. Ceram. Soc.* 78[3] (1995) 797-800.
7. J.J. Petrovic, M.I. Pena, and H.H. Kung, *J. Am. Ceram. Soc.* 80[5] (1997) 1111-1116.
8. J.J. Petrovic, M.I. Pena, I.E. Reimanis, M.S. Sandlin, S.D. Conzone, H.H. Kung, and D.P. Butt, *J. Am. Ceram. Soc.* 80[12] (1997) 3070-3076.
9. Ming-yuan Kao, *J. Am. Cer. Soc.* 76 (1993) 2879-2083.
10. J.J. Petrovic, and R.E. Honnell, *J. Mat. Sci. Lett.* 9 (1990) 1083-1084.
11. E.L. Courtright, *Mat. Sci. Eng. A261* (1999) 53-63.
12. K. Niihara, and Y. Suzuki, *Mat. Sci. Eng. A261* (1999) 6-15.
13. Y. Suzuki, T. Sekino, T. Hamasaki, K. Ishizaki, and K. Niihara, *Mat. Lett.* 37 (1998) 143-148.
14. L.J. Neergaard, and J.J. Petrovic, in *Ceramic Engineering & Science Proceedings* (The American Ceramic Society, Westerville, Ohio, 1995), p. 137
15. B.-R. Zhang, F. Marino, and V.M. Sglavo, *J. Am. Cer. Soc.* 81[5] (1998) 1344-1348.
16. K. Yanada, and N. Kamiya, *Mat. Sci. Eng. A261* (1999) 270-277.
17. H. Klemm, K. Tangermann, C. Schubert, and W. Hermel, *J. Am. Cer. Soc.* 79[9] (1996) 2429-2435.
18. A. Bellosi, and G.N. Babini, in *Key Engineering Materials* (Trans Tech Publications, Switzerland, 1994), Vol. 89-91 p. 117.

19. A. Bellosi, and G.N. Babini, in Key Engineering Materials (Trans Tech Publications, Switzerland, 1999) Vol. 161-163 p. 203.
20. G.R. Anstis, P. Chantikul, B.R. Lawn, and D.B. Marshall, J. Am. Ceram. Soc. 64[9] (1981) 533-538.
21. D.G. Munz, J.L. Shannon, and R.T. Bubsey, International Journal of Fracture, Vol. 16 (1980) R137-R141.
22. Z. Hashin, "Elasticity of Ceramic Systems", in Proceedings of the Third International Symposium on Ceramic Microstructure: their Analysis, Significance and Production (John Wiley & Sons Inc. Publishers, New York, USA, 1968) p. 313.
23. M.S. Sakaguchi, N. Murayama, Y. Kodama, and F. Wakai, J. Mat. Sci. Lett. 10 (1991) 282-284.
24. N.E. Dowling, in Mechanical behavior of materials (Prentice-Hall, Inc., Englewood Cliffs, New Jersey, 1993) p. 182.
25. A. Kelly, and N.H. Macmillan, in Strong solids (Clarendon Press, Oxford, 1986) p. 392.
26. K.-H. Zum Gahr, in Microstructure and wear of materials - Tribology Series (Elsevier, The Netherlands, 1987), Vol. 10, p. 36.
27. D.J. Green, and P.S. Nicholson, in Fracture Mechanics of Ceramics, (Plenum Press, New York, 1978), Vol. 4, pp. 945-960.
28. B.-N. Kim, M. Watanabe, M. Enoki, and T. Kishi, Engineering Fracture Mechanics 59 (1998) 289-303.
29. Stress Intensity Factors Handbook (Ed. by Y. Murakami, Pergamon Press, Oxford, 1987), Vol. 1, p. 42.
30. B.R. Zhang, F. Marino, V.M. Sglavo, and S. Gialanella, Materials Science and Engineering A239-240 (1997) 503-506.
31. D.K. Hale, J. Mat. Sci. 11 (1976) 2105-2141.
32. J.F. Shackelford, and W. Alexander, in Material Science and Engineering Handbook (Third ed., CRC Press, USA, 2001) p. 487.
33. D.S. McLachlan, M. Blaszkiewicz, and R.E. Newnham, J. Am. Ceram. Soc. 73[8] (1990) 2187-2203.